The Astrophysical Journal, 641:795–800, 2006 April 20

THE POLYCYCLIC AROMATIC HYDROCARBON EMISSION DEFICIT IN LOW-METALLICITY GALAXIES—A *SPITZER* VIEW

B. O'Halloran,[1] S. Satyapal,[1,2] and R. P. Dudik[1]
Received 2005 August 31; accepted 2005 December 15

ABSTRACT

Archival observations of 18 starburst galaxies that span a wide range in metallicity reveal for the first time a correlation between the ratio of emission-line fluxes of [Fe II] at 26 μm and [Ne II] at 12.8 μm and the 7.7 μm PAH strength, with the [Fe II]/[Ne II] flux ratio decreasing with increasing PAH strength. We also find a strong correlation between the [Fe II]/[Ne II] flux ratio and the host galaxy metallicity, with the flux ratio decreasing with increasing metallicity. Since [Fe II] emission has been linked primarily to supernova shocks, we attribute the high [Fe II]/[Ne II] ratios in low-metallicity galaxies to enhanced supernova activity. We consider this to be a dominant mechanism for PAH destruction, rather than grain destruction in photoionized regions surrounding young massive stars. We also consider whether the extreme youth of the low-metallicity galaxies is responsible for the lack of PAH emission.

Subject headings: galaxies: starburst — galaxies: stellar content — infrared: galaxies — ISM: lines and bands

1. INTRODUCTION

Recent surveys in the UV and IR (Galliano et al. 2005; Engelbracht et al. 2005; Hogg et al. 2005; Madden et al. 2006; Rosenberg et al. 2006) have highlighted the importance of low-metallicity galaxies for the investigation of vigorous episodes of star formation. In particular, nearby blue compact dwarf (BCD) galaxies provide evidence that isolated, small, low-metallicity galaxies may experience high star formation levels in the present epoch (Hopkins et al. 2002). Since the advent of *Infrared Space Observatory* (*ISO*) it has been known that very low metallicity ($Z \ll 1$) galaxies show very little in the way of polycyclic aromatic hydrocarbonate (PAH; Puget & Leger 1989) emission in the mid-IR (Madden 2000; Sturm et al. 2000). PAH emission is thought to be linked to star-forming activity (Roussel et al. 2001); UV photons from massive young stars excite the PAH carriers, and therefore trace the extent of star formation.

Low PAH luminosity in strongly star forming galaxies is contrary to what has been seen previously by *ISO* surveys; in starbursts, ubiquitous strong PAH emission was detected (see review by Genzel & Cesarsky 2000). However, from *ISO* data it has been tentatively noted that as the metallicity of the galaxy increases, so too does the strength of the PAH emission (Sturm et al. 2000; Haas et al. 2002). This begs the question, what causes the PAH emission deficiency in low-metallicity galaxies? Is it a case of PAH carriers being destroyed, or is the PAH deficiency intrinsic?

Hirashita et al. (2002) note that dust destruction is the dominant interstellar medium (ISM) process when the metallicity of a low-metallicity galaxy such as a BCD reaches $12 + \log(\mathrm{O/H}) \lesssim 8$. Furthermore, recent work by Galliano et al. (2005) suggests that the small size of ISM grains emitting in the mid- and far-IR may be due to destruction by shock waves from supernovae (SNe) in these galaxies. In low-metallicity galaxies, star formation is dominated by massive stars ($M_{\mathrm{init}} \geq 35\ M_{\odot}$), and high SN rates are expected in galaxies experiencing very recent massive star formation (Mas-Hesse & Kunth 1999). An extremely high SN rate and/or extremely energetic SNe (with up to 10^{52} ergs being released into the ISM; Galama et al. 1998) from very massive stars could very well be responsible for the lack of PAHs in low-metallicity galaxies. In this scenario, strong SN shocks propagating into the ISM may be the culprit responsible for the PAH deficiency.

In order to investigate this question, a tracer of SN activity is required. The mid-IR [Fe II] lines offer an ideal extinction-insensitive tool to probe the SN activity in actively star forming galaxies. Iron is an abundant refractory element; however, it is highly depleted from the gas phase of the interstellar medium in galaxies as a result of condensation onto dust grains (e.g., de Boer et al. 1987). Forbidden line emission from low ionization states of Fe is greatly enhanced behind hydrodynamic shock fronts, where grain processing can result in near solar gas-phase Fe abundances. The near-infrared [Fe II] lines at 1.257 and 1.644 μm have been widely used to trace the SN content in galaxies (e.g., Greenhouse et al. 1991, 1997; Calzetti 1997). Likewise, the $a\ ^6D(7/2–9/2)$ transition of [Fe II] near 26 μm can also be used as a relatively pure tracer of SN activity. The low excitation potential corresponding to the transition (550 K) may in fact imply that emission from the mid-IR lines is longer lasting than emission from the higher excitation potential near-IR lines, which are thought to persist only up to 10^4 yr (Oliva et al. 1989) after a SN explosion. This feature, coupled with emission from [Ne II] at 12.8 μm, which traces emission from very massive young stars, could be used to determine the SN shock emission relative to the present ionizing photon production rate. [Ne II] is a robust indicator of the ionizing photon rate in dust-enshrouded starburst galaxies. For galaxies dominated by typical stellar UV fields, a simple linear proportionality between the [Ne II] luminosity and the Lyman continuum luminosity is expected from photoionization models (Thornley et al. 2000). Measurements of the [Fe II]/[Ne II] emission-line ratio in starburst galaxies could thus provide a sensitive measure of the supernova content of galaxies (Greenhouse et al. 1991, 1996; Moorwood & Oliva 1988) and hence an estimate of the degree of grain processing and destruction. Furthermore, an increased SN rate or shock wave intensity, indicated by a higher [Fe II]/[Ne II], would be highly suggestive that in low-metallicity galaxies destruction by SN shocks is responsible for the absence of PAHs.

Given the availability of high spatial and spectral resolution data in the mid-IR from *Spitzer* of nuclear regions of starbursts (where massive stars are located), we can search for [Fe II]

[1] Department of Physics and Astronomy, George Mason University, Fairfax, VA, 22030.
[2] Presidential Early Career Award Scientist.

TABLE 1
Sample Parameters

Target (1)	R.A. (2)	Decl. (3)	Hubble Type (4)	Distance (Mpc) (5)	Metallicity ($Z_\odot$) (6)	L(IR) ($L_\odot$) (7)	Metallicity Reference (8)
I Zw 18	09 34 02.0	55 14 28	cI BCD	10.6	7.2	$\leq 3.2 \times 10^8$	1
Tol 65	12 25 46.9	−36 14 01	H II	38.0	7.6	$\leq 5.0 \times 10^8$	2
Mrk 25	10 03 51.8	59 26 10	E/S0 H II	42.1	7.8	7.5×10^9	3
Mrk 170	11 26 50.4	64 08 17	Pec	13.8	7.9	2.9×10^8	4
UM 448	11 42 12.4	00 20 03	Sb pec; Sbrst H II	78.4	8.0	7.2×10^{10}	1
II Zw 40	05 55 42.6	03 23 33	BCD/Sbc	11.1	8.1	3.5×10^9	1
Mrk 930	23 31 58.3	28 56 50	Sbrst	77.3	8.1	2.6×10^{10}	5
NGC 4670	09 32 10.1	21 30 03	SB(s)0/a pec: BCDG	15.1	8.2	1.9×10^9	6
IC 342	03 46 48.5	68 05 46	SAB(rs)cd H II	3.0	8.3	2.5×10^9	7
NGC 7793	23 58 58.9	03 38 05	Sbc	3.2	8.7	4.4×10^8	8
NGC 4194	12 14 09.5	54 31 37	IBm pec; BCG H II	34.4	8.8	7.7×10^9	9
NGC 253	00 47 33.1	−25 17 18	SAB(s)c; H II Sbrst	3.4	8.9	2.6×10^{10}	1
He 2-10	08 36 15.2	−26 24 34	I0? pec Sbrst	12.3	8.9	5.3×10^9	1
NGC 7714	23 36 14.1	02 09 19	SB(s)b:pec; H II	39.4	8.9	5.2×10^{10}	1
NGC 3049	09 54 49.6	09 16 18	SB(rs)ab; H II Sbrst	21.1	9.0	3.9×10^9	10
NGC 1482	03 54 38.9	−20 30 09	SA0+ pec sp H II	27.1	9.1	7.1×10^{10}	11
M82	09 55 52.2	69 40 47	I0; Sbrst H II	2.9	9.2	2.9×10^{10}	12
NGC 2903	09 32 10.1	21 30 03	SB(s)d H II	7.8	9.3	7.9×10^9	1

Notes.—Units of right ascension are hours, minutes, and seconds, and units of declination are degrees, arcminutes, and arcseconds. Col. (1): Common source names. Col. (2): Right ascension. Col. (3): Declination. Col. (4): Galaxy morphology in terms of Hubble type. Col. (5): Distance of object in megaparsecs. Col. (6): Metallicity of galaxy in terms of solar metallicity, where metallicity $= 12 + \log(\mathrm{O/H})$. Col. (7): Infrared luminosity of galaxy in terms of solar luminosity, where $L(\mathrm{IR}) = 1.8 \times 10^{-14}(13.48 f_{12} + 5.16 f_{25} + 2.58 f_{60} + f_{100})$. Col. (8): Sources for metallicity values.

References.—(1) Engelbracht et al. 2005; (2) Izotov et al. 2004; (3) Hopkins et al. 2002; (4) Petrosian & Turatto 1986; (5) Izotov & Thuan 1999; (6) Lisenfeld & Ferrara 1998; (7) Crosthwaite et al. 2001; (8) Kong & Cheng 1999; (9) Garnett 2002; (10) Gonzalez-Delgado 2002; (11) Parmentier et al. 2003; (12) Hameed & Devereux 1999.

emission from nearby starbursts and compare the [Fe II]/[Ne II] ratio as a function the strength of the PAH emission to see whether any correlation exists. Such a diagnostic, using data from galaxies of known metallicity, will allow us to determine whether SN-driven shocks play an important role in the PAH emission deficit in low-metallicity galaxies.

2. OBSERVATIONS AND DATA ANALYSIS

A total of 18 starburst galaxies of known metallicity from optical studies (see references in Table 1 for sources) were selected from the *Spitzer* archive to form the core sample. The full list of targets is given in Table 1, and they are listed in terms of increasing metallicity. These galaxies range in metallicity from extremely low (such as I Zw 18, with $Z/Z_\odot = 1/50$) to supersolar metallicity ($\gtrsim 1\ Z_\odot$) galaxies such as M82 and NGC 7714. To differentiate between low- and high-metallicity galaxies, we use a metallicity $[12 + \log(\mathrm{O/H})]$ cutoff value of 8.85, just less than solar, with the majority of the low-metallicity galaxies having values less than 8.3. The galaxies range widely in morphology from blue compact dwarfs such as I Zw 18 to spirals such as NGC 7714 and IC 342. None of the galaxies in our sample are known to harbor active galactic nuclei (AGNs). This is important, as PAH destruction can occur close to an AGN due to the hard ionization environment (Sturm et al. 2000). In addition, [Fe II] emission can be elevated in galaxies harboring AGNs (e.g., Sturm et al. 2000). One possible exception is NGC 7714, which is optically classified as a LINER (Thomas et al. 2002). However, the lack of [Ne V] emission at 14 and 24 μm and the absence of any evidence for an obscured AGN by recent *Chandra* imaging (Brandl et al. 2004; Smith et al. 2005) strongly suggest that NGC 7714 is a pure starburst, and it is therefore included in our sample. Most of the targets are nearby, with only Mrk 25 (42.1 Mpc), Mrk 930 (77.3 Mpc), and UM 448 (78.4 Mpc) greater than 40 Mpc away (assuming a value of $H_0 = 71$ km s^{-1} Mpc^{-1}), allowing detections of the comparatively weak [Fe II] emission.

We extracted low- and high-resolution archival spectral data from the Short-Low (SL; 5.2–14.5 μm), Short-High (SH; 9.9–19.6 μm), and Long-High (LH; 18.7–37.2 μm) modules of the *Spitzer* Infrared Spectrograph (IRS). The data sets were derived from a number of *Spitzer* Legacy and Guaranteed Time Observation programs released to the *Spitzer* Data Archive and consisted of either spectral mapping or staring observations. We obtained fluxes for the nuclear positions only from the mapping observations. All the staring observations were centered on the galaxy's nucleus.

The data were preprocessed by the *Spitzer* Science Center (SSC) data reduction pipeline, version 12.0,[3] before being downloaded. Further processing was done within the IDL-based IRS data reduction and analysis package SMART, version 5.5.2 (Higdon et al. 2004). The high-resolution spectra were extracted using the full-aperture extraction method along the diffraction orders. For the low-resolution spectra, the spectra were extracted using the interactive column extraction option, which is similar to the method used in the SSC pipeline and allowed for definition of a source as well as a manual definition of the background. For both high- and low-resolution spectra, the ends of each order, where the noise increases significantly, were manually clipped, as were hot pixels.

Fluxes were extracted for the emission lines [Ne II] at 12.8 μm and [Fe II] at 26 μm using the SMART interactive line-fitting tool, along with the 7.7 μm PAH feature. The 7.7 μm PAH strength was determined according to the prescription adopted in a number of previous studies (Rigopoulou et al. 1999; Forster Schreiber

[3] *Spitzer* Observers Manual, http://ssc.spitzer.caltech.edu/documents/som.

TABLE 2
Flux, Luminosity, and Ratio Data

Target (1)	F([Ne II]) at 12.8 μm (W cm^{-2}) (2)	F([Ne III] at 15.6 μm (W cm^{-2}) (3)	[Ne III]/[Ne II] Ratio 15.6/12.8 μm (4)	F([Fe II]) at 26.0 μm (W cm^{-2}) (5)	[Fe II]/[Ne II] Ratio 26.0/12.8 μm (6)	L([PAH]) 7.7 μm Feature (W) (7)	PAH 7.7 μm Peak/Continuum (8)
I Zw 18	$4.32 \pm 0.10 \times 10^{-22}$	$4.02 \pm 0.58 \times 10^{-22}$	0.95	$7.20 \pm 2.10 \times 10^{-22}$	1.67	1.1×10^{27}	1.33
Tol 65	$3.29 \pm 0.39 \times 10^{-22}$	$7.23 \pm 0.50 \times 10^{-22}$	2.20	$5.40 \pm 0.66 \times 10^{-22}$	1.64	1.0×10^{28}	1.57
Mrk 25	$1.30 \pm 0.04 \times 10^{-20}$	$5.65 \pm 0.19 \times 10^{-21}$	0.44	$8.10 \pm 1.60 \times 10^{-21}$	0.62	2.8×10^{29}	2.75
Mrk 170	$7.39 \pm 1.56 \times 10^{-22}$	$1.39 \pm 0.06 \times 10^{-21}$	1.88	$6.53 \pm 0.75 \times 10^{-22}$	0.88	1.1×10^{27}	1.60
UM 448	$1.82 \pm 0.05 \times 10^{-20}$	$1.20 \pm 0.02 \times 10^{-20}$	0.66	$5.73 \pm 1.09 \times 10^{-21}$	0.32	9.6×10^{29}	1.89
II Zw 40	$5.90 \pm 0.16 \times 10^{-21}$	$1.70 \pm 0.05 \times 10^{-20}$	2.88	$1.51 \pm 0.41 \times 10^{-21}$	0.26	2.4×10^{28}	2.17
Mrk 930	$2.65 \pm 0.19 \times 10^{-21}$	$9.40 \pm 0.09 \times 10^{-21}$	3.55	$1.40 \pm 0.32 \times 10^{-21}$	0.53	5.2×10^{29}	2.42
NGC 4670	$5.90 \pm 0.44 \times 10^{-21}$	$1.70 \pm 0.14 \times 10^{-20}$	3.82	$3.84 \pm 0.52 \times 10^{-21}$	0.66	2.2×10^{28}	2.27
IC 342	$4.58 \pm 0.15 \times 10^{-19}$	$3.24 \pm 0.24 \times 10^{-20}$	0.07	$7.70 \pm 0.03 \times 10^{-20}$	0.17	1.1×10^{29}	2.60
NGC 7793	$3.30 \pm 0.17 \times 10^{-21}$	$9.70 \pm 0.57 \times 10^{-22}$	2.94	$1.01 \pm 0.28 \times 10^{-21}$	0.31	5.9×10^{27}	2.70
NGC 4194	$1.15 \pm 0.05 \times 10^{-19}$	$4.93 \pm 0.08 \times 10^{-20}$	0.43	$1.24 \pm 0.31 \times 10^{-20}$	0.17	6.0×10^{30}	3.20
NGC 253	$3.04 \pm 0.07 \times 10^{-18}$	$2.21 \pm 0.22 \times 10^{-19}$	0.07	$3.08 \pm 0.13 \times 10^{-19}$	0.16	3.0×10^{30}	2.93
He 2-10	$2.80 \pm 0.04 \times 10^{-19}$	$1.12 \pm 0.04 \times 10^{-19}$	0.40	$2.30 \pm 0.09 \times 10^{-20}$	0.08	2.2×10^{30}	4.05
NGC 7714	$1.08 \pm 0.03 \times 10^{-19}$	$7.95 \pm 0.08 \times 10^{-20}$	0.74	$1.30 \pm 0.16 \times 10^{-20}$	0.12	9.6×10^{30}	3.20
NGC 3049	$3.00 \pm 0.08 \times 10^{-20}$	$3.95 \pm 0.24 \times 10^{-21}$	0.13	$9.70 \pm 0.18 \times 10^{-21}$	0.32	8.0×10^{29}	2.70
NGC 1482	$3.90 \pm 0.07 \times 10^{-19}$	$3.20 \pm 0.32 \times 10^{-20}$	0.10	$1.70 \pm 0.07 \times 10^{-20}$	0.04	1.7×10^{31}	4.53
M82	$4.69 \pm 0.22 \times 10^{-19}$	$8.58 \pm 0.05 \times 10^{-20}$	0.18	$7.10 \pm 0.23 \times 10^{-20}$	0.08	2.2×10^{30}	3.91
NGC 2903	$8.52 \pm 0.04 \times 10^{-19}$	$7.95 \pm 0.36 \times 10^{-20}$	0.09	$8.50 \pm 0.06 \times 10^{-20}$	0.10	4.3×10^{29}	4.54

Notes.—Col. (1): Common source names. Col. (2): Flux of the 12.8 μm [Ne II] fine-structure line in watts per cm squared. Col. (3): Flux of the 15.6 μm [Ne III] fine-structure line in watts per cm squared. Col. (4): Ratio of the [Ne III] and [Ne II] fine-structure lines. Col. (5): Flux of the 26.0 μm [Fe II] fine-structure line in watts per cm squared. Col. (6): Ratio of the [Fe II] and [Ne II] fine-structure lines. Col. (7): Luminosity of the 7.7 μm PAH feature in watts. Col. (8): Ratio of the flux density of the peak of the 7.7 μm PAH feature to the flux density of the continuum at 7.7 μm.

et al. 2004). Here, the continuum was determined at the center of the 7.7 μm feature, with the continuum determined using a first-order linear fit to the 5.9 and 9.5 μm bandpass. The PAH strength was then calculated as the ratio of the 7.7 μm feature peak intensity to the underlying continuum. The silicate absorption feature at 9.7 μm was not prominent in any of our spectra. We therefore do not consider it to significantly affect the strength of the 7.7 μm PAH feature.

The use of three separate apertures for the SL, SH, and LH modules raises the issue of aperture effects on the extracted fluxes, and by extension, any derived correlations. Nuclear star formation, responsible for the bulk of the PAH emission and mid-IR continuum in the vast majority of galaxies, originates from the central few hundred parsecs (e.g., Surace & Sanders 1999; Scoville et al. 2000; Satyapal et al. 2005). However, given the different morphologies and physical scales within the sample, it is quite plausible that for some of our sample at least, IR emission and associated star formation extend farther than the central few hundred parsecs, and thus a larger proportion of the mid-IR and far-IR (FIR) emission may fall outside the IRS aperture beams.

In order to determine whether aperture corrections are required, we used Multiband Imaging Photometer for *Spitzer* (MIPS) 70 μm images to trace the spatial extent of the FIR emission. If the FIR was not contained within the Long-High slit (covering roughly the central kiloparsec), we considered the source to be extended; otherwise the source was considered compact. For 66% of the sample (all of the low-metallicity and one of the high-metallicity galaxies), the FIR emission is fully contained within the IRS aperture beams, and for these galaxies aperture corrections are not likely to be significant. For the remaining galaxies, a quick inspection of the MIPS 70 μm images reveals that the FIR is more extended than the IRS aperture. In § 3.1.1, we discuss the possible impact of the resulting aperture variations on our results. The line fluxes, PAH luminosities, and fine-structure line ratio data for the sample are given in Table 2.

3. RESULTS AND DISCUSSION

3.1. *Behavior of the* [Fe II]/[Ne II] *Ratio*

3.1.1. *Does the* [Fe II]/[Ne II] *Ratio Vary with PAH Strength?*

In order to investigate how the strength of SN shocks relative to the massive star population varies with the strength of the PAH emission, we plot the [Fe II]/[Ne II] emission-line ratio versus the 7.7 μm PAH peak to continuum ratio for each galaxy in Figure 1. It is immediately apparent that a strong correlation exists between the [Fe II]/[Ne II] ratio and the PAH strength; as the PAH strength increases, the [Fe II]/[Ne II] ratio drops. Interestingly, a

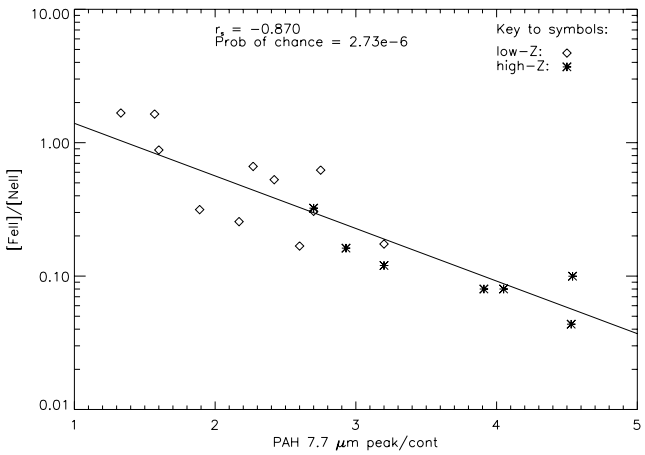

Fig. 1.—Plot of the [Fe II]/[Ne II] ratio as a function of the PAH strength for the sample. The Spearman rank coefficient (r_s) of −0.870 and the very low probability of chance correlation value (P_s) of 2.73×10^{-6} confirm that a highly significant anticorrelation exists between the [Fe II]/[Ne II] ratio and the PAH strength. This strong correlation suggests that supernova-driven shocks are the dominant mechanism responsible for the PAH deficiency in low-metallicity galaxies; this is discussed further in § 3.1.

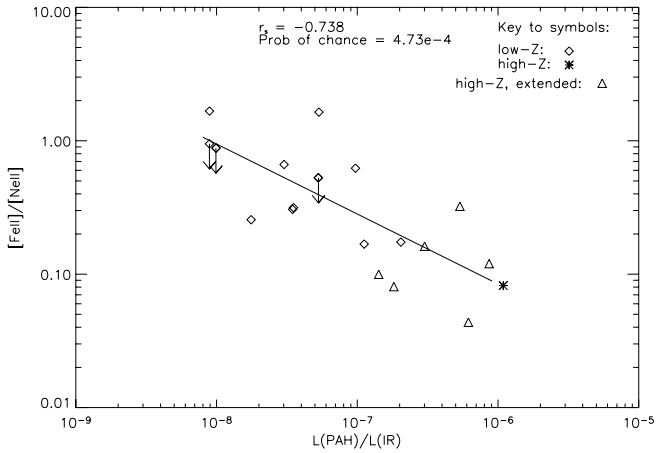

FIG. 2.—Plot of the [Fe II]/[Ne II] ratio as a function of the PAH/IR luminosity ratio. The Spearman rank coefficient (r_s) of −0.738 and the very low probability of chance correlation value (P_s) of 4.73×10^{-4} confirm that a strong anticorrelation exists between the [Fe II]/[Ne II] ratio and the PAH/IR luminosity ratio. The extended high-metallicity sources are indicated by the triangles. This correlation, along with that in Fig. 1, suggests that supernova-driven shocks are the dominant mechanism responsible for the PAH deficiency in low-metallicity galaxies.

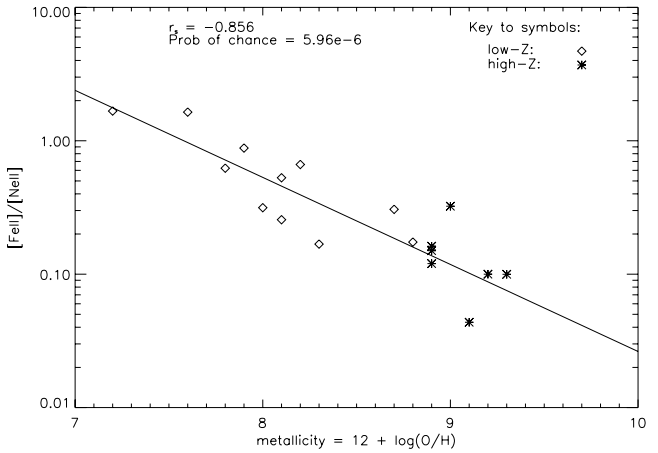

FIG. 3.—Plot of the [Fe II]/[Ne II] ratio as a function of the galaxy metallicity. The Spearman rank coefficient (r_s) of −0.856 and the very low probability of chance correlation value (P_s) of 5.96×10^{-6} show that a very robust anticorrelation exists between the [Fe II]/[Ne II] ratio and the metallicity of the galaxy. This strong anticorrelation, along with those in Figs. 1 and 2, would firmly suggest that supernova-driven shocks are the dominant mechanism responsible for the PAH deficiency in low-metallicity galaxies.

clear divide exists between low- and high-metallicity galaxies on the plot. Employing a Spearman rank correlation analysis (Kendall & Stuart 1976) to assess the statistical significance of this trend yields a correlation coefficient (r_s) of −0.870 between [Fe II]/[Ne II] and the PAH strength with a probability of chance correlation (P_s) of 2.73×10^{-6}, indicating a significant anticorrelation. The Spearman rank correlation technique has the advantage of being nonparametric and robust to outliers and does not presuppose a linear relation.

Since the PAH strength can also be dependent on the strength of the mid-IR dust continuum, we can attempt to decouple this effect by plotting the [Fe II]/[Ne II] ratio versus the ratio of the 7.7 μm PAH feature luminosity and the total IR luminosity (Fig. 2), which also includes emission from much larger dust grains. Although the *Infrared Astronomical Satellite* (*IRAS*) aperture is larger than those on IRS, it has been widely demonstrated that the 12–100 μm fluxes in star-forming galaxies are dominated by emission from the nuclear regions of the galaxy that also give rise to the PAH emission (Imanishi 2003; Rodriguez-Ardila & Viegas 2003). A preliminary analysis of the 70 μm MIPS images of our sample of galaxies shows that for six of the seven high-metallicity starbursts included in Figure 2 (M82, NGC 7714, NGC 3049, NGC 1482, NGC 253, and NGC 2903), the FIR emission is more extended than the IRS aperture through which the PAH emission is measured. Since these aperture variations can potentially result in systematic errors in the PAH/FIR flux ratio, we have distinguished extended sources from compact sources in Figure 2. Using the Spearman rank correlation technique again, a similar but weaker ($r_s = -0.738$; $P_s = 4.73 \times 10^{-4}$) correlation is found. Both plots confirm that a strong relationship exists between the PAH strength and the strength of the [Fe II]/[Ne II] ratio. The MIPS images of our sample of galaxies will be discussed in a follow-up work.

3.1.2. *Does the* [Fe II]/[Ne II] *Ratio Vary with Metallicity?*

Since it has been previously suggested from *Spitzer* imaging and *ISO* camera (ISOCAM) circular variable filter (CVF) spectra (Engelbracht et al. 2005; Madden et al. 2006; Rosenberg et al. 2006) that PAH emission also varies with metallicity, we can also explore whether the [Fe II]/[Ne II] ratio varies in a similar fashion, given the link between PAH emission and the [Fe II]/[Ne II] emission seen in Figure 1. In Figure 3, we see a strong anticorrelation ($r_s = -0.856$; $P_s = 5.96 \times 10^{-6}$), with the [Fe II]/[Ne II] ratio dropping with increasing metallicity. Again as in Figure 1, we see a clear separation in the [Fe II]/[Ne II] ratio between galaxies of low and high metallicity.

We must state that the correlations we see here are derived from compact starburst regions, and we must be careful in extrapolating this result to suggest that there is a global lack of PAHs in low-metallicity galaxies. Quiescent dwarf galaxies, which are not currently undergoing strong star formation or numerous SN events, may exhibit stronger PAH emission than that seen in the starburst dwarf galaxies in our sample. For quiescent dwarfs, diffuse star formation provides a mechanism for the excitation of the PAH carriers, excited through extended low-level star formation and by lower mass stars from earlier bursts. In support of this, using fluxes from Infrared Array Camera (IRAC) and MIPS imaging, Engelbracht et al. (2005) note a large scatter of PAH emission to 24 μm continuum ratios for a number of dwarf galaxies, suggesting that a contribution is made to the overall PAH emission from quiescent regions outside the nuclear starburst regions, which would enhance PAH emission even within low-metallicity galaxies.

3.2. *What Causes the Lack of PAH Emission in Low-Metallicity Galaxies?*

3.2.1. *UV Radiation or SN Shocks?*

UV radiation from the massive O star population may play an important role in PAH destruction in low-metallicity galaxies due to the hard ionizing radiation field surrounding these stars (Plante & Sauvage 2002). In Figure 4, we plot the [Ne III] 15.5 μm /[Ne II] 12.8 μm ratio versus the PAH strength for our sample. The [Ne III]/[Ne II] ratio is a robust extinction- and abundance-insensitive indicator of the hardness of the radiation field surrounding massive young stars (Thornley et al. 2000). Although Figure 4 shows a significant correlation ($r_s = -0.612$; $P_s = 6.88 \times 10^{-3}$), there is considerable scatter, and the correlation is weaker than the correlation displayed in Figure 1. This correlation confirms a similar diagnostic presented in Madden et al. (2006) for a range of objects of varying morphology and spatial scale that include H II regions and spiral, starburst, and dwarf galaxies.

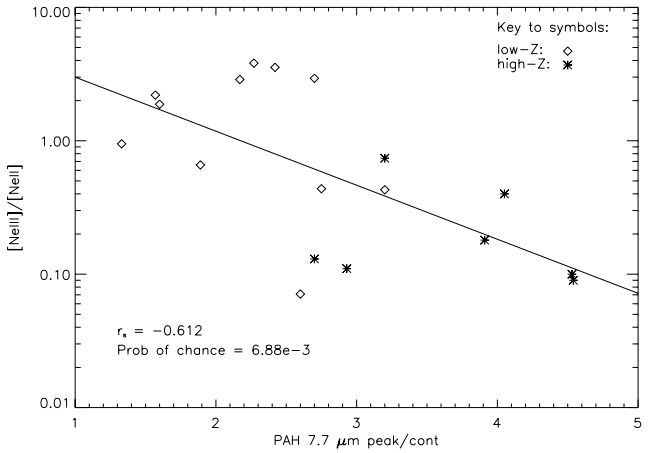

FIG. 4.—Plot of the [Ne III]/[Ne II] ratio as a function of the PAH strength. Although there is a significant correlation ($r_s = -0.612$; $P_s = 6.88 \times 10^{-3}$), there is considerable scatter and the correlation is weaker than the correlation displayed in Fig. 1. This suggests that grain destruction by SN-driven shocks likely plays a more pronounced role than grain destruction within H II regions in terms of PAH carrier destruction, given the strength of the correlations in Figs. 1–3.

The strength of the correlation in Figure 4 in relation to that in Figure 1 suggests that PAH destruction by SN-driven shocks likely plays a more pronounced role than grain destruction from UV radiation within H II regions. Indeed, there is observational precedence for suggesting that SN-driven shocks play a pivotal role in the destruction of PAHs. Using ISOCAM-CVF spectra, Reach et al. (2002) did not detect PAH emission within either ionic or molecular shocks in a number of Galactic supernova remnants including 3C 391, despite strong PAH features detected in the spectra of the preshock region and also in nearby regions not affected by the SN remnant. Furthermore, the shocked emission shows no significant continuum rise at mid-IR wavelengths. This rise is normally seen in interstellar dust spectra, including those of quiescent regions such as reflection nebulae, and has been attributed to the presence of very small dust grains (VSGs; Desert et al. 1990; Madden et al. 2006). The lack of PAH emission within shocked regions has also been noted in other Galactic SN remnants such as G11.2−0.3 and Kes 69, based on IRAC color ratios (Reach et al. 2006). The lack of aromatic features or rising continuum in the mid-IR spectrum of 3C 391 suggests that both the PAH carriers and VSGs are destroyed by SN shocks. The lack of PAHs in our sample of low-metallicity galaxies, plus a lack of rising mid-IR continua for the low-metallicity sample, suggests very strongly that SN shocks play a dominant role in the PAH emission deficit in these objects, and indeed for the state of the ISM as a whole.

In order to further clarify and disentangle the contributions that UV radiation surrounding young stars and SN shocks make to the destruction of PAH carriers and to the evolution of the ISM in low-metallicity galaxies, a follow-up high-resolution spectral mapping survey of low-metallicity galaxies using IRS is critical. Such a high spatial resolution spectroscopic survey will provide further insight into the physics of grain and aromatic feature destruction in high-ionization starburst and shock front environments.

3.2.2. *Lack of ISM Enrichment by PAHs*

An alternate scenario for the low PAH emission in low-metallicity galaxies is that due to the extreme youth of these galaxies, not enough time has elapsed for stars below 8 $M_\odot$ to move off the main sequence (MS) to become asymptotic giant branch (AGB) stars. These evolved objects are considered to be the primary source for PAHs (Morgan & Edmunds 2003). An AGB star consists of a degenerate C/O core surrounded by a very extended convective atmosphere, from which mass is lost via a dense and dusty outflow at rates of 10^{-8} to 10^{-4} $M_\odot$ yr^{-1} and at expansion velocities of 5–30 km s^{-1} (Matsuura et al. 2005). PAH carriers from AGB stars take ~200 Myr to be injected into the ISM, when ~4 $M_\odot$ stars evolve off the MS (Dwek 2005), thus requiring several generations of star formation to enrich the ISM with PAH carriers.

However, AGB stars have been detected even in the galaxy with the lowest known metallicity, I Zw 18 (Izotov & Thuan 2004), and the age of the AGB population (~500 Myr) is more than long enough for injection of PAHs into the ISM, and for the ISM to become PAH enriched. However, modeling by Morgan & Edmunds (2003) suggests that despite the presence of AGB stars, a timescale of up to 1 Gyr is required to enrich the ISM with PAHs to the level we see in higher metallicity galaxies. Nevertheless, the presence of AGB stars plus the expected level of PAH enrichment after 500 Myr (from the models of Morgan and Edmunds 2003) indicate that we should see higher PAH emission than has been detected in low-metallicity galaxies such as I Zw 18. Given the high [Fe II]/[Ne II] ratios for low-metallicity galaxies, it would be plausible to suggest that shocks from SNe further depress PAH emission in these galaxies through destruction of the PAH carriers. Such a scenario may help to explain the lack of PAH emission even in galaxies with advanced AGB populations. The lack of PAH emission within SN shocks such as those within the Galactic SN remnant 3C 391 (Reach et al. 2002) would strongly enhance the plausibility of this scenario.

3.3. *Is There Evidence of a Variation in the Upper Mass Limit with Increasing Metallicity?*

From discussions of the evolution of fine-structure line ratios in §§ 3.1 and 3.2.1, we note that the decrease in the strength of the fine-structure line ratios with higher metallicity is consistent with the hardness of the ionizing radiation in the starburst increasing with decreasing metallicity (Campbell et al. 1986; Madden et al. 2006; Wu et al. 2006). It has been suggested that the formation of massive stars is directly related to lower metallicities within the ISM, with a larger Jeans mass being formed due to a drop in the cooling efficiency of the primordial gas (Bromm et al. 2002) leading to a higher ionization environment within the starburst regions. Given the proclivity for such low-metallicity objects to produce such massive stars, it would be interesting to determine whether the decrease in the [Ne III]/[Ne II] ratio with higher metallicity is indicative of a variation in the upper mass limit of the initial mass function (IMF) with increasing metallicity. Theoretical studies predict that the production of very massive stars in high-metallicity galaxies is suppressed through feedback from previous stellar generations (Moy et al. 2001; Rigby & Rieke 2004). The drop in the [Ne III]/[Ne II] ratio with increasing metallicity and PAH strength would suggest a lack of very massive stars (with initial masses greater than 40 $M_\odot$) being formed and going on to produce supernovae as the ISM evolves through feedback from earlier generations. In support of this scenario, photoionization work by Rigby & Rieke (2004) and Martin-Hernandez et al. (2005) attributes low excitation ratio values to high-mass, solar-metallicity starbursts forming fewer massive stars through feedback into the ISM. However, since the [Ne III]/[Ne II] ratio is dependent on both the upper mass cutoff ($M_{\rm upper}$) and the age of the stellar population (e.g., Leitherer et al. 1999), it is difficult to decouple one effect from the other. Further detailed modeling using stellar population

synthesis codes coupled with photoionization codes using a large number of line diagnostics could help constrain $M_{\rm upper}$.

4. CONCLUSIONS

Using archival spectral data from *Spitzer*, we undertook a survey of 18 starburst galaxies in order to determine whether SN shocks are responsible for the PAH deficiency in low-metallicity galaxies. Using the emission-line ratio of [Fe II] at 26 μm to [Ne II] at 12.8 μm plotted against the PAH strength, we found a strong anticorrelation, with the [Fe II]/[Ne II] ratio decreasing with increasing PAH emission. Similar correlations were found when comparing the [Fe II]/[Ne II] ratio to the PAH/IR luminosities and metallicity. Since [Fe II] emission has been linked primarily to SN shocks, we attribute the high [Fe II]/[Ne II] ratios in low-metallicity galaxies to enhanced SN activity and consider this to be the dominant mechanism for PAH destruction, rather than grain destruction in photoionized regions surrounding young massive stars. We also consider whether the extreme youth of the low-metallicity galaxies is responsible for the lack of PAH emission. While the age of the known AGB populations in our low-metallicity sample galaxies is less than the time required for full PAH enrichment of the ISM, we argue that SN shocks (as evidenced by the high [Fe II]/[Ne II] ratios and SN rates) further depress the PAH emission. We conclude that while SN shock destruction of the PAH carriers may not be fully responsible for the lack of PAH emission, it remains a prime culprit for the lack of PAH emission in low-metallicity galaxies.

This work is based on archival data obtained with the *Spitzer Space Telescope*, which is operated by the Jet Propulsion Laboratory, California Institute of Technology under a contract with NASA. We wish to thank J. Weingartner for helpful comments and guidance, and of course the referee for providing comments and feedback on our original submission.

REFERENCES

Brandl, B. R., et al. 2004, ApJS, 154, 188
Bromm, V., Coppi, P. S., & Larson, R. 2002, ApJ, 564, 23
Calzetti, D. 1997, AJ, 113, 162
Campbell, A., Terlevich, R., & Melnick, J. 1986, MNRAS, 223, 811
Crosthwaite, L. P., Turner, J. L., Hurt, R. L., Levine, D. A., Martin, R. N., & Ho, P. T. P. 2001, AJ, 122, 797
de Boer, K. S., Jura, M. A., & Shull, J. M. 1987, in Exploring the Universe with the *IUE* Satellite, ed. Y. Kondo (Dordrecht: Reidel), 485
Desert, F. X., Boulanger, F., & Puget, J. L. 1990, A&A, 237, 215
Dwek, E. 2005, in AIP Conf. Proc. 761, The Spectral Energy Distributions of Gas-Rich Galaxies: Confronting Models with Data, ed. C. C. Popescu & R. J. Tuffs (New York: AIP), 103
Engelbracht, C. W., Gordon, K. D., Rieke, G. H., Werner, M. W., Dale, D. A., & Latter, W. B. 2005, ApJ, 628, L29
Forster Schreiber, N. M., Roussel, H., Sauvage, M., & Charmandaris, V. 2004, A&A, 419, 501
Galama, T. J., et al. 1998, Nature, 395, 670
Galliano, F., Madden, S. C., Jones, A. P., Wilson, C. D., & Bernard, J.-P. 2005, A&A, 434, 867
Garnett, D. 2002, ApJ, 581, 1019
Genzel, R., & Cesarsky, C. J. 2000, ARA&A, 38, 761
Gonzalez-Delgado, R. M. 2002, ApJ, 580, 824
Greenhouse, M. A., Woodward, C. E., Thronson, H. A., Jr., Rudy, R. J., Rossano, G. S., Erwin, P., & Puetter, R. C. 1991, ApJ, 383, 164
Greenhouse, M. A., et al. 1996, BAAS, 28, 1404
———. 1997, ApJ, 485, 438
Haas, M., Klaas, U., & Bianchi, S. 2002, A&A, 385, L23
Hameed, S., & Devereux, N. 1999, AJ, 118, 730
Higdon, S. J. U., et al. 2004, PASP, 116, 975
Hirashita, H., Tajiri, T., & Kamaya, H. 2002, A&A, 388, 439
Hogg, D. W., Tremonti, C. A., Blanton, M. R., Finkbeiner, D. P., Padmanabhan, N., Quintero, A. D., Schlegel, D. J., & Wherry, N. 2005, ApJ, 624, 162
Hopkins, A. M., Sculte-Ladbeck, R. E., & Drozdovsky, I. O. 2002, AJ, 124, 862
Imanishi, M. 2003, ApJ, 599, 918
Izotov, Y. I., Papaderos, P., Guseva, N. G., Fricke, K. J., & Thuan, T. X. 2004, A&A, 421, 539
Izotov, Y. I., & Thuan, T. X. 1999, ApJ, 511, 639
———. 2004, ApJ, 616, 768
Kendall, M., & Stuart, A. 1976, The Advanced Theory of Statistics, Vol. 2 (New York: Macmillian)
Kong, X., & Cheng, F. Z. 1999, A&A, 351, 477
Leitherer, C., et al. 1999, ApJS, 123, 3
Lisenfeld, U., & Ferrara, A. 1998, ApJ, 496, 145
Madden, S. C. 2000, NewA Rev., 44, 249
Madden, S. C., Galliano, F., Jones, A. P., & Sauvage, M. 2006, A&A, 446, 877
Martin-Hernandez, N. L., Schaerer, D., & Sauvage, M. 2005, A&A, 429, 449
Mas-Hesse, J. M., & Kunth, D. 1999, A&A, 349, 765
Matsuura, M., et al. 2005, A&A, 434, 691
Moorwood, A. F. M., & Oliva, E. 1988, A&A, 203, 278
Morgan, H. L., & Edmunds, M. G. 2003, MNRAS, 343, 427
Moy, E., Rocca-Volmerange, B., & Fioc, M. 2001, A&A, 365, 347
Oliva, E., Moorwood, A. F. M., & Danziger, I. J. 1989, A&A, 214, 307
Parmentier, G., de Grijs, R., & Gilmore, G. 2003, MNRAS, 342, 208
Petrosian, A., & Turatto, M. 1986, A&AS, 65, 349
Plante, S., & Sauvage, M. 2002, AJ, 124, 1995
Puget, J. L., & Leger, A. 1989, ARA&A, 27, 161
Reach, W. T., Rho, J., Jarrett, T. H., & Lagage, P. O. 2002, ApJ, 564, 302
Reach, W. T., et al. 2006, AJ, 131, 1479
Rigby, J. R., & Rieke, G. H. 2004, ApJ, 606, 237
Rigopoulou, D., Spoon, H. W. W., Genzel, R., Lutz, D., Moorwood, A. F. M., & Tran, Q. D. 1999, AJ, 118, 2625
Rodriguez-Ardila, A., & Viegas, S. M. 2003, MNRAS, 340, L33
Rosenberg, J. L., Ashby, M. L. N., Salzer, J. J., & Huang, J.-S. 2006, ApJ, 636, 742
Roussel, H., Sauvage, M., Vigroux, L., & Bosma, A. 2001, A&A, 372, 427
Satyapal, S., Dudik, R. P., O'Halloran, B., & Gliozzi, M. 2005, ApJ, 633, 86
Scoville, N. Z., et al. 2000, AJ, 119, 991
Smith, B. J., Struck, C., & Nowak, M. A. 2005, AJ, 129, 1350
Sturm, E., Lutz, D., Tran, D., Feuchtgruber, H., Genzel, R., Kunze, D., Moorwood, A. F. M., & Thornley, M. D. 2000, A&A, 358, 481
Surace, J. A., & Sanders, D. B. 1999, ApJ, 512, 162
Thomas, H. C., Dunne, L., Clemens, M. C., Alexander, P., Eales, S., & Green, D. A. 2002, MNRAS, 329, 747
Thornley, M. D., Förster Schreiber, N. M., Lutz, D., Genzel, R., Spoon, H. W. W., Kunze, D., & Sternberg, A. 2000, ApJ, 539, 641
Wu, Y., Charmandaris, V., Hao, L., Brandl, B. R., Bernard-Salas, J., Spoon, H. W. W., & Houck, J. R. 2006, ApJ, 639, 157